MRS Advances (2025) 10:2188–2192
https://doi.org/10.1557/s43580-025-01391-9

ORIGINAL PAPER

Synthesis and oxidation of Ru-doped UO_2

Damien Prieur[1,2] · Jean-François Vigier[3] · Viktoria Baumann[3] · Karin Popa[3] · Emanuele De Bona[1,3] · Herwin Hein[3] · Kathy Dardenne[4] · Jörg Rothe[4] · Aaron Beck[4] · Tonya Vitova[5] · Marco Cologna[3]

Received: 9 July 2025 / Accepted: 5 September 2025 / Published online: 15 September 2025

Abstract

Ru-doped UO_2 materials were synthesized via a sol–gel method and the resulting compounds were subjected to an oxidative heat treatment at 1000 °C. Both as-synthesized and oxidized materials were characterized coupling microscopy, diffraction and spectroscopic techniques. A detailed structural description of the studied compounds is provided. The oxidation of UO_2 to U_3O_8 is complete within the investigated atmosphere and Ru is oxidized to volatile oxide forms.

Introduction

The fission reaction of one heavy atom, such as ^{235}U and ^{239}Pu, is associated with the formation of lighter elements called fission products (FPs) [1]. During irradiation in a nuclear power plant reactor, the oxide fuel becomes doped with tens of FP elements, the concentration of which increases continuously. Besides the volatility of some FPs (Xe, Kr), the presence of FPs prominently affects the physical and chemical properties of the fuel (valence state, crystallographic form, migration behavior, thermodynamic stability, etc.).

During temporary off-normal irradiation conditions (*e.g.,* loss of flow accidents), the spent fuel can be in contact with an oxidizing atmosphere, which results in its progressive oxidation with the successive formation of U_3O_7/U_4O_9 and then of U_3O_8 [2]. The final state depends on several parameters, such as the oxygen partial pressure of the atmosphere conditions, the moisture and the temperature. If the atmosphere is sufficiently oxidizing, some FP metals can then form highly volatile FP oxide species [3, 4]. In addition, these conditions enhance a faster cladding corrosion and ultimately its failure. This latter scenario implies that fuel and FPs are released in the surrounding environment.

Among the fission products, ruthenium is of particular interest due to its ability to form volatile oxide compounds in oxidizing conditions; for example, RuO_4 can volatilize already at temperature as low as 170 °C. In addition, Ru is a very hazardous component because of its chemical toxicity and radiotoxicity. *In operando*, Ru, like other noble metal FPs (*e.g.,* Rh, Pd, Tc, Mo), forms separate metallic phases which are considered as moderately volatile species [5].

In this context, this work aims at synthesizing Ru-doped UO_2 materials and characterizing the as-synthesized and oxidized compounds.

Experimental

Synthesis process

Uranium dioxide beads were prepared at JRC with the sol gel method [6] as described in the SI. The beads were calcined at 600 °C in air for 2 h (to burn the organics) and in Ar/H_2 for 4 h (to reduce uranium oxide) at a heating rate of 200 °C h^{-1}. The beads were then infiltrated with a $RuCl_3$ water solution to reach a nominal composition of 0.5 and 5 mol% Ru

✉ Damien Prieur
damien.prieur@esrf.fr

✉ Karin Popa
karin.popa@ec.europa.eu

1 Institute of Resource Ecology, Helmholtz-Zentrum Dresden-Rossendorf, 01328 Dresden, Germany

2 The Rossendorf Beamline at ESRF-The European Synchrotron, CS40220, 38043 Grenoble Cedex 9, France

3 Joint Research Centre (JRC), European Commission, Karlsruhe, Germany

4 Radionuclide Speciation Department, Institute for Nuclear Waste Disposal (INE), Karlsruhe Institute of Technology (KIT), 76344 Eggenstein-Leopoldshafen, Germany

5 Advanced Spectroscopy in F-Element Chemistry Department, Institute for Nuclear Waste Disposal (INE), Karlsruhe Institute of Technology (KIT), 76344 Eggenstein-Leopoldshafen, Germany

(based on U content, *i.e.,* respectively, 0.2 and 2 *wt.%* of Ru in UO_2), dried overnight and calcined in Ar/6%H_2 for 4 h at 600 °C with a heating rate of 200 °C h^{-1}. Some of the pure UO_2 (*i.e.,* 0 mol% Ru) beads were also calcined in the same way for reference purposes. The beads were mixed with ca. 0.5 *wt.%* zinc stearate, pressed at 400 MPa and sintered at 1600 °C for 6 h with a heating rate of 200 °C h^{-1} in an Ar/6%H_2 mixture. The sintered densities were derived from the pellet geometrical dimensions. After characterization, the as-synthesized compounds were subjected to an oxidative treatment, under air at 1000 °C for 4 h.

XRD, SEM, TGA and XAS techniques (U M_{IV} HERFD-XANES and U L_{III} EXAFS) were employed for the characterization. The *ATHENA* software was used to extract EXAFS oscillations from the raw absorption spectra. Curve fitting with the *ARTEMIS* software was performed in k^3 space [7]. Details are given in the SI.

Results and discussion

Characterization of the calcined powders

After calcination, XRD was performed on the resulting powder and only a cubic UO_{2+x} phase was observed. No Ru phase was identified. According to the XRD patterns (Figure S1), the UO_{2+x} peaks are broad due to the high strain in the material. The strain broadening being high compared to the crystal size broadening, the crystal size could not be precisely determined but is at least a few tens of nanometers. According to the derived lattice parameter, these materials are hyperstoichiometric as their values are smaller than the expected value for stoichiometric $UO_{2.00}$ (*i.e.,* 5.4713 Å) [8]. Their deviations from the stoichiometry have been assessed and reported in Table S1.

Characterization of the as-sintered pellets

As detailed in the experimental section, the calcined powders were then pressed and sintered at 1600 °C for 6 h. Table S2 shows that the mass loss during sintering ranged from 0.90(5) to 1.10(5) *wt.%*, accounting probably for residual organics, adsorbed water and hydroxyl groups and hyperstoichiometry of the starting powder. The mass loss is independent of the Ru content, suggesting that no Ru is lost during the sintering step, as one would expect in a reducing atmosphere. The sintered densities are ranging from 91.8(5) % to 93.1(5) %.

The sintered pellets were polished and observed by scanning electron microscopy (Figure S2). The samples doped with ruthenium show some large areas with low porosity. The higher the Ru content, the more such high-density regions appear. Within the same cross section, such dense, Ru-rich areas are not homogeneously distributed, possibly due to some inhomogeneity in the doping of the starting doped beads. The microstructure of the pure UO_2 sample is more homogenous, although some areas with smaller porosity adjacent to areas with bigger porosity are present, as evidenced from the SEM images at high magnification. Some cracks appear in the Ru-doped samples, but only when the nominal Ru concentration is 5 mol%. Possible causes of the cracks are the residual thermal stresses created upon cooling by the mismatch in the thermal expansion coefficient of UO_2 and Ru and possibly the stresses during densification due to the different sintering kinetics of the Ru-rich and Ru-poor phases.

Figure S3 presents the XRD patterns of the sintered compounds; narrower peaks than for the calcined powders are observed. This is expected in reason of both grain growth and strain decrease. One can observe that both URu0.5% and URu5% as-sintered compounds exhibit a Fm-3 m fluorite-type phase with lattice parameters equal to 5.471(1) Å (Table 1).

These values are in fair agreement with a stoichiometric $UO_{2.00}$. The non-defective fluorite structure is also confirmed by both HERFD-XANES and EXAFS measurements, which are presented in Figs. 1 and 2, respectively.

Indeed, comparing the U M_{IV} HERFD-XANES spectra of the two as-sintered compounds with the $UO_{2.00}$ reference, one can see that they are well aligned and that there is no shift toward higher energy. It indicates that the oxidation state of U is purely tetravalent, as in a stoichiometric $UO_{2.00}$. In addition, the interatomic distances derived from EXAFS also corroborate this as they are in fair agreement

Table 1 Phase composition and crystallographic data of the as-sintered and oxidized materials

Sample	Phase	Weight ratio (%)	Lattice parameter (Å)			Angle (°)			Space group
			a	b	c	α	β	γ	
URu0.5%	UO_2	100	5.471(1)	5.471(1)	5.471(1)	90	90	90	Fm-3m-225
URu0.5%_ox1000°C	U_3O_8	100	6.721(1)	11.957(1)	4.147(1)	90	90	90	C2mm-38
URu5%	UO_2	99	5.471(1)	5.471(1)	5.471(1)	90	90	90	Fm-3m-225
	Ru	1	2.702(1)	2.702(1)	4.284(1)	90	90	120	P63/mmc-194
URu5%_ox1000°C	U_3O_8	100	6.723(1)	11.952(1)	4.147(1)	90	90	90	C2mm-38

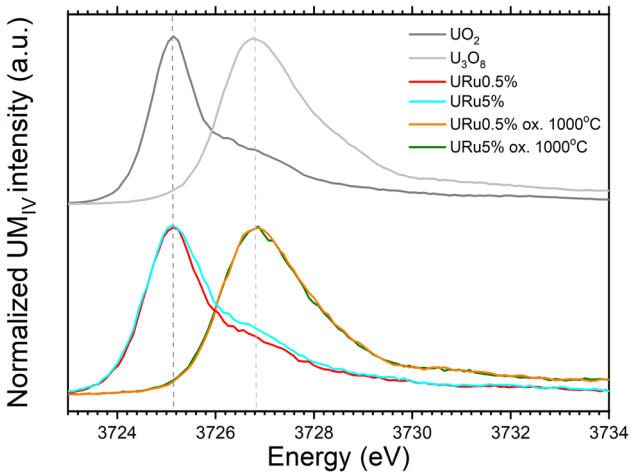

Fig. 1 U M_{IV} HERFD-XANES spectra of as-sintered and oxidized URu0.5% and URu5% compared with UO_2 and U_3O_8 references [9, 10, 11, 12]

with the expected values for a stoichiometric $UO_{2.00}$ (*cf.* Table 2).

The Ru content in the sample evaluated by XRD is in fair agreement with the expected values. In URu0.5% (~0.2 *wt.%* Ru), no Ru phase is observed, as the amount is below the typical detection limit of XRD (typically around 1 *wt.%*). In the case of URu5% (~2 *wt.%* Ru), Ru metallic phase is detected, with a phase ratio obtained from Rietveld refinement is ~1%, in fair agreement with the nominal value, considering the large errors at such low concentrations. The lattice parameter of the sintered pellets is independent of the Ru content, suggesting that Ru is not present as a solute in the UO_2 matrix.

Characterization of the oxidized pellets

The as-sintered pellets were then heat-treated under air at 1000 °C for 4 h. As could have been expected from the U–O phase diagram [9], two α-U_3O_8 orthorhombic phases are achieved for both oxidized URu0.5% and URu5% compounds. Indeed, both XRD (Figure S4) and EXAFS (Fig. 2) show that both fitted interatomic distances and lattice parameters are close to the literature values [10]. In addition, the U M_{IV} HERFD-XANES data indicates that the U valences in the samples match those of our U_3O_8 reference. In these thermal conditions, *i.e.,* air at 1000 °C, one can conclude that the oxidation from UO_2 to U_3O_8 is complete regardless of the amount of Ru [13–15].

Furthermore, in the URu5% sample, one should note that the Ru metallic phase, present before in the as-synthesized compound, is not present after this oxidative treatment. One can assume that either the weight ratio is below the detection limit or that the Ru has been accommodated by the U_3O_8 structure or that the Ru volatilizes during the heating treatment. To check this assumption, TGA measurements were performed under air at 1600 °C on both UO_2 and URu5% (Figure S5). In the case of UO_2, an important weight gain associated to the oxidation of UO_2 into U_3O_8 is observed. For the URu5% sample, the gain weight is even larger, which can be attributed to the oxidation to U_3O_8 on one hand and to the oxidation of metal Ru to RuO_2 or RuO_3 on the other hand. Then, a specific weight loss is observed for URu5% compared to UO_2 sample, which can be attributed to the volatilization of Ru. The difference between the two TGA curves seems in agreement with an initial Ru content in the sample slightly below 1 *wt.%*. The TGA data show that the onset

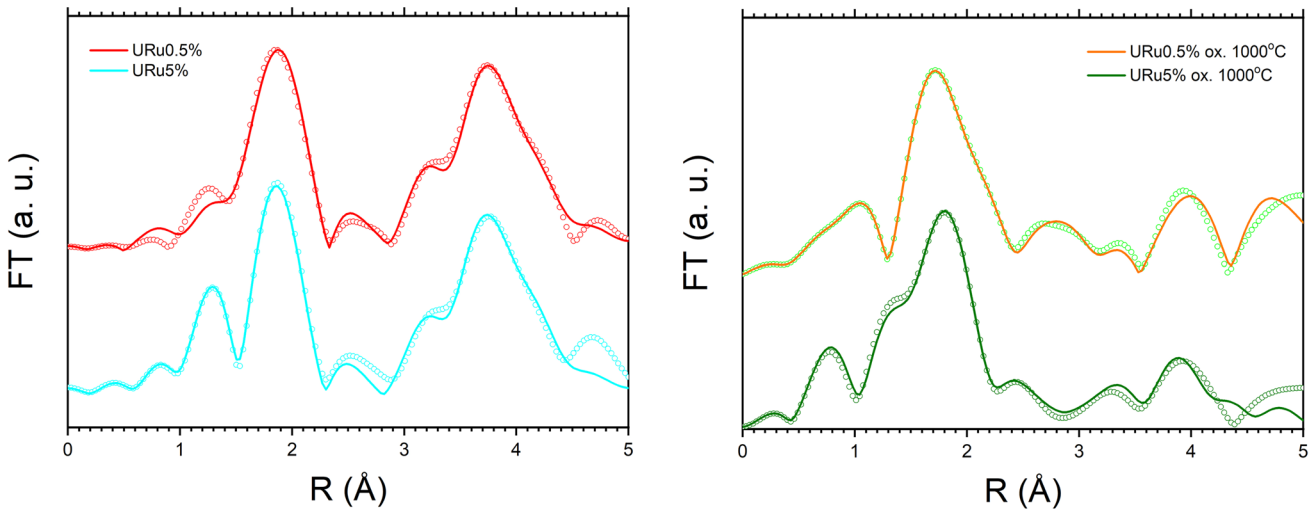

Fig. 2 Experimental and modelled Fourier transformed k^3-weighted EXAFS spectra. (left: as-sintered material, right: after calcination under air at 1000 °C)

Table 2 Crystallographic parameters derived from EXAFS. The interatomic distances *R*, the coordination numbers *N*, and the Debye–Waller factors σ^2 were derived from the EXAFS spectra. The uncertainties are the numbers in round brackets

Sample	Space group	Shell	N	*R* (Å)	σ^2 (Å^2)	Rf (%)
URu0.5%	*Fm-3 m*	U-O	8	2.354(5)	0.006(1)	1.5
		U-U	12	3.87(1)	0.004(1)	
		U-O	24	4.47(1)	0.008(1)	
URu0.5%_1000°C	*C2mm*	U-O	2	2.00(1)	0.004(1)	3.1
		U-O	4	2.21(1)	0.008(1)	
		U-O	1	2.60(1)	0.012(1)	
		U-U	2	3.72(1)	0.006(1)	
		U-U	2	3.85(1)	0.010(1)	
		U-U	4	4.15(2)	0.007(1)	
URu5%	*Fm-3 m*	U-O	8	2.352(5)	0.005(1)	1.7
		U-U	12	3.86(1)	0.004(1)	
		U-O	24	4.46(1)	0.009(1)	
URu5%_ox1000°C	*C2mm*	U-O	2	2.01(1)	0.005(1)	3.2
		U-O	4	2.22(1)	0.007(1)	
		U-O	1	2.60(1)	0.015(1)	
		U-U	2	3.72(1)	0.006(1)	
		U-U	2	3.83(1)	0.013(1)	
		U-U	4	4.16(2)	0.008(1)	

of oxidation of Ru is seen already at 600 °C [11], while volatilization begins just below 1000 °C.

Conclusions

In this work, we synthesized by sol–gel method Ru-doped UO_2 compounds at different concentrations. After sintering in a reducing atmosphere, UO_2-like fluorite structures were achieved in all studied compounds. The oxidation state of U is purely tetravalent, as in a stoichiometric $UO_{2.00}$, independently from the Ru content. Also, the lattice parameter is independent from Ru content, suggesting that Ru is not present in the lattice as a solute, but only as a precipitate at grain boundaries. A Ru metallic phase has been evidenced by XRD in the sample containing initially 5 mol% of Ru. After oxidation in air at 1000 °C, we evidenced that U_3O_8-like structures were obtained, showing that a total oxidation from UO_2 to U_3O_8 occurred during this oxidative step. The ruthenium metallic phase is oxidized from 600 °C and begins the volatilization as oxide while approaching 1000 °C. This study yields a deeper understand of the behaviour of Ru and finally spent fuel under oxidizing conditions.

Supplementary Information The online version contains supplementary material available at https://doi.org/10.1557/s43580-025-01391-9.

Acknowledgments We acknowledge the KIT light source for provision of instruments at their beamlines and we would like to thank the Institute for Beam Physics and Technology (IBPT) for the operation of the storage ring, the Karlsruhe Research Accelerator (KARA). We are grateful to both JRC and INE teams for their help during the sample preparation and the synchrotron measurements, respectively.

Author contributions Conceptualization: DP, EDB, MC; methodology: DP, JFV, EDB, KD, JR, TV, MC; formal analysis and investigation: DP, JFV, VB, KP, EDB, HH, KD, JR, AB, TV, MC; resources: DP, KP, KD, JR, TV, MC; writing—original draft: DP, EDB, MC; writing—review and editing: DP, JFV, VB, KP, EDB, HH, KD, JR, AB, TV, MC; funding acquisition: DP, TV; supervision: DP, KP, TV, MC; project administration: DP, MC.

Funding Not applicable.

Data availability The data that support the findings of this study are available upon reasonable request.

Declarations

Conflict of interest The authors declare that they have no known competing financial interests or personal relationships that could have appeared to influence the work reported in this paper.

References

1. B.J. Lewis, W.T. Thompson, F.C. Iglesias, Fission product chemistry in oxide fuels, in *Comprehensive nuclear materials*. (Elsevier, Oxford, 2012), pp.515–546
2. R.J. McEachern, A. Taylor, A review of the oxidation of uranium dioxide at temperatures below 400 °C. J. Nucl. Mater. **254**, 87–121 (1998)
3. M.A. Mansouri, D.R. Olander, Fission product release from trace irradiated UO2+x. J. Nucl. Mater. **254**, 22–33 (1998)
4. E. De Bona, K. Popa, O. Walter, C. Hennig, A.C. Scheinost, D. Prieur, Oxidation of micro- and nanograined UO2 pellets by in situ synchrotron X-ray diffraction. Inorg. Chem. **61**(4), 1843–1850 (2022)
5. C. Mun, L. Cantrel, C. Madic, Review of literature on ruthenium behavior in nuclear power plant severe accidents. Nucl. Technol. **156**, 332–346 (2006)
6. M. Cologna, V. Tyrpekl, M. Ernstberger, S. Stohr, J. Somers, Submicrometre grained UO2 pellets consolidated from sol gel beads using spark plasma sintering (SPS). Ceram. Int. **42**, 6619–6623 (2016)
7. B. Ravel, M. Newville, ATHENA, ARTEMIS, HEPHAESTUS: data analysis for X-ray absorption spectroscopy using IFEFFIT. J. Synchrotron Radiat. **12**, 537–541 (2005)
8. G. Leinders, T. Cardinaels, K. Binnemans, M. Verwerft, Accurate lattice parameter measurements of stoichiometric uranium dioxide. J. Nucl. Mater. **459**, 135–142 (2015)
9. K.O. Kvashnina, Y.O. Kvashnin, S.M. Butorin, Role of resonant inelastic X-ray scattering in high-resolution core-level spectroscopy of actinide materials. J. Electron Spectrosc. Relat. Phenom. **194**, 27–36 (2014)
10. G. Leinders, R. Bes, J. Pakarinen, K.O. Kvashnina, M. Verwerft, Evolution of the uranium chemical state in mixed-valence oxides. Inorg. Chem. **56**, 6784–6787 (2017)
11. G. Kauric, O. Walter, A. Beck, B. Schacherl, O. Dieste Blanco, J.-F. Vigier, E. Zuleger, T. Vitova, K. Popa, Synthesis and characterization of nanocrystalline U1-xPuxO2(+y) mixed oxides. Mater. Today Adv. **8**, 100105:1–6 (2020)
12. J.-F. Vigier, D. Freis, O. Walter, O. Dieste Blanco, D. Bouëxière, E. Zuleger, N.V.T. Palina, R.J.M. Konings, K. Popa, Synthesis and characterization of homogeneous (U, Am)O2 and (U, Pu, Am)O2 nanopowders. CrystEngComm **24**, 6338–6348 (2022)
13. C. Guéneau, A. Chartier, L. Van Brutzel, Thermodynamic and thermophysical properties of the actinide oxides, in *Comprehensive nuclear materials*. (Elsevier, Oxford, 2012), pp.21–59
14. B.O. Loopstra, Neutron diffraction investigation of U3O8. Acta Crystallogr. A **17**, 651–564 (1964)
15. S. Gupta, M.D.R. Sinha, R. Jangir, A. Bose, P. Gupta, M.K. Swami, M.H. Modi, Study of oxidation behaviour of Ruthenium thin film after thermal annealing in oxygen environment. Thin Solid Films **764**, 139606:1-139606:7 (2023)